Self-imaging through incoherent to coherent conversion

María del Carmen Lasprilla A.*
Alexandra Agra Amorim†
Myrian Cristina Tebaldi
Néstor A. Bolognini
Centro de Investigaciones Ópticas, CIOp (CONICET, CIC)
Casilla de Correo 124
1900 La Plata, Argentina
E-mail: postmaster@ciop.edu.ar

Abstract. The self-imaging phenomenon is realized by utilizing an incoherent to coherent converter. For this purpose, a photorefractive BSO crystal that becomes uniformly birefringent due to an external applied voltage is employed. Then, an incoherently illuminated one-dimensional grating that locally modulates the induced birefringence is registered. In the readout process, a linearly polarized plane wave from a He-Ne laser is utilized. The ellipticity of the light exiting the crystal will be determined according to the local birefringence. Then, after passing through a polarizer, the coherent output will reproduce the incoherent input. In this way, under free propagation, coherent replicas of the grating will be obtained.

Subject terms: self-imaging; real-time image processing; photorefractive crystals.

Paper 19085 received Aug. 18, 1995; accepted for publication Oct. 23, 1995.

1 Introduction

When a periodic transparency (for instance, a Ronchi grating) is illuminated with a monochromatic collimated beam, the grating amplitude transmittance is periodically reproduced along the propagation direction. These replicas under free propagation are called self-images.[1] The spatial frequencies of self-imaging objects have to be discrete and located on the so-called Montgomery rings.[2]

A Ronchi grating of spatial period d fulfills the mentioned condition and therefore generates self-images. It should be mentioned that lateral periodicity of an object is sufficient but not necessary for self-imaging to occur. When the grating transparency is illuminated with a plane wave of wavelength λ, the Fresnel diffraction patterns located at distances $z_T = 2d^2 n/\lambda$ ($n = 1,2,3,...$) from the grating reproduce the input grating.[2,3]

Furthermore, the diffraction patterns located between the transparency and the first self-image are repeated between any two successive self-images. That is, the diffracted field is longitudinally periodic.

Photorefractive crystals such as the sillenites combine real-time response, reversibility, and high sensitivity in the visible portion of the spectrum that make them very attractive for many optical information processing and related applications.[4] In this work, an incoherent to coherent converter arrangement that utilizes a sillenite photorefractive crystal (BSO) to encode a periodic transparency is proposed. To this end, the write-in step is detailed in the following section. Afterwards, we discuss the coherent readout process that allows the replicas of the input to be produced.

2 Theoretical Analysis

Let us consider the experimental setup schematized in Fig. 1. A transparency O, which consists of a grating of binary amplitude with an opening ratio equal to 0.5, is illuminated with a white light source S through the condenser lens L_1. An image of unit magnification of the transparency is obtained in the crystal by means of the lens L_2. The directions $\langle \bar{1}10 \rangle$, $\langle 001 \rangle$, and $\langle 110 \rangle$ of the crystal coincide with the X, Y, and Z axes, respectively (laboratory axes).

The crystal exhibits the linear electro-optic effect. Thus, if a voltage V is applied between $(\bar{1}10)$ faces separated a distance L_x, it becomes uniformly birefringent due to the external field $E_a = V/L_x$. The slow and fast index-induced optical axes are at ± 45 deg with respect to the $\langle \bar{1}10 \rangle$ direction. The crystal has a strong photoconductivity in the range of wavelength between 400 and 550 nm. A filter centered at 530 nm ($\Delta\lambda$ ± 3 nm) is placed in front of the white-light source. Under these conditions the light pattern received by the crystal, that is, the Ronchi grating projected by the lens L_2, will create photocharges that will drift due to the external field E_a into the dark regions, where they are trapped. These charges develop a space-charge field that partially compensates the external field in the illuminated areas. In this way, the induced birefringence will be locally modulated according to the light pattern, producing a local change in the ellipticity of the transmitted light.

In order to compute the resulting total internal field E in the crystal, the Kukhtarev equations are employed.[5,6] Considering that the input pattern is a one-dimensional light distribution, a single-spatial-variable approach to these equations is possible:

$$J(x,t) = qD\frac{\partial N(x,t)}{\partial x} + q\mu N(x,t)\left[E_{sc}(x,t) + \frac{V}{L_x}\right], \tag{1}$$

$$\frac{\partial N(x,t)}{\partial t} = g(x) - \frac{N(x,t) - N_D}{\tau} + \frac{1}{e}\frac{\partial J(x,t)}{\partial x}, \tag{2}$$

*Current affiliation: Universidad Industrial de Santander, Departamento de Física, A.A. 678, Bucaramanga, Colombia.
†Current affiliation: Instituto Superior de Engenharia do Porto, Departamento de Física, 4200 Porto, Portugal.

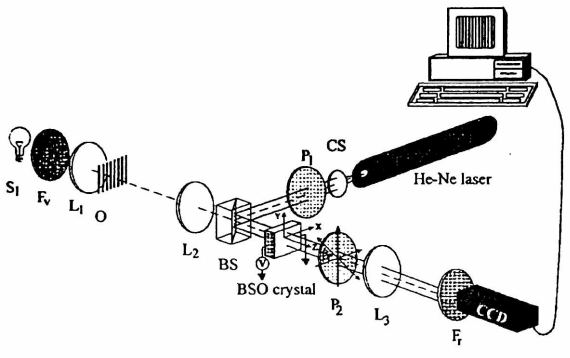

Fig. 1 Experimental setup. S: incoherent source; L_1 and L_2: lenses; F_v: filter centered at 530 nm; O: input transparency (Ronchi grating); BS: beamsplitter; CS: collimated system; F_r: filter centered at 630 nm, P_1 and P_2: polarizers.

where x and t are spatial and temporal variables, respectively, J is the current density, and N is the total free-carrier concentration, which includes the contribution due to the light pattern and the contribution N_D of the free charges in the dark. Furthermore, e is the electron charge, μ is the mobility, τ is the free-carrier lifetime, and D is the diffusion coefficient.

The usual assumption is made that the generation rate $g(x)$ is proportional to the light pattern $I_i(x)$ received by the crystal. That is, $g(x)=g_0 I_i(x)/I_0$, where $I_i(x)/I_0$ is the normalized light intensity and g_0 is proportional to the highest intensity value I_0. Also, the photoinduced space charge field E_{sc} must fulfill

$$\int_{-L_x/2}^{L_x/2} E_{sc}(x,t)\,dx=0. \tag{3}$$

The gradient contribution $\partial N/\partial x$ in the diffusion term of Eq. (1) can be neglected because of the smooth variation of $I_i(x)$ on a microscopic scale. Furthermore, in the steady-state situation $\partial N/\partial t=0$, a constant current density J is of concern.

Under these conditions, from Eqs. (1), (2), and (3), the following total internal field results:

$$E(x)=E_{sc}(x)+\frac{V}{L_x}=\frac{J}{q\mu N(x)}=\frac{V}{KN(x)}, \tag{4}$$

where the expression for $N(x)$ is

$$N(x)=N_D\left[1+\frac{\tau g_0}{N_D}I_i(x)\right]=N_D[1+GI_i(x)] \tag{5}$$

and $G=\tau g_0/N_D$. The value of K is obtained as

$$K=\int_{-L_x/2}^{L_x/2}\frac{dx}{N(x)}. \tag{6}$$

For this configuration, the calculated expression for the modulated birefringence is

$$\delta n(x)=n_0^3 r_{41}E(x), \tag{7}$$

where r_{41} is the electro-optic coefficient and n_0 is the refractive index without induced field.

In the readout or reconstruction process, a collimated Y-direction linearly polarized plane wave from a He-Ne laser is utilized. In order to avoid destructive readout of the stored information, a wavelength that is outside of the spectral sensitivity range of the crystal is employed. Then, let us consider the light amplitude transmitted by the crystal in the readout process. It will be necessary to compute the produced changes in the light ellipticity.

The BSO crystal exhibits rotatory power per unit length $\rho(\lambda)$ (where λ is the wavelength employed for readout), which combines with the induced birefringence modulation $\delta n(x)$. This means that when light of a given ellipticity enters the crystal, in order to evaluate the change in the polarization state, both effects must be computed.

In this case, following the Jones formalism,[7] the following transfer matrix[4] W_C of the crystal written in the coordinate system of the two induced axes results:

$$W_C(x)=\begin{pmatrix}\cos\Delta(x)-i\sin\psi(x)\sin\Delta(x) & -\cos\psi(x)\sin\Delta(x)\\ \cos\psi(x)\sin\Delta(x) & \cos\Delta(x)+i\sin\psi(x)\sin\Delta(x)\end{pmatrix} \tag{8}$$

and

$$\begin{pmatrix}A_x'\\ A_y'\end{pmatrix}=R\left(-\frac{\pi}{4}\right)W_C(x)R\left(\frac{\pi}{4}\right)\begin{pmatrix}0\\ 1\end{pmatrix}=\begin{pmatrix}\sin\Delta(x)\,\exp[i\psi(x)]\\ \cos\Delta(x)\end{pmatrix} \tag{9}$$

where R is the rotation matrix and A_x' and A_y' are the respective output amplitudes in the laboratory axes, and

$$\Delta(x)=L_z\left[\rho^2+\frac{\varphi^2(x)}{4}\right]^{1/2},\quad \psi(x)=\tan^{-1}\left[\frac{\varphi(x)}{2\rho}\right] \tag{10}$$

with

$$\varphi(x)=\frac{2\pi}{\lambda}\delta n(x)=\frac{2\pi}{\lambda}n_0^3 r_{41}E(x). \tag{11}$$

In the experimental setup that is schematized in Fig. 1, the polarizer P_1 is placed with its pass plane parallel to the Y axis, and the polarizer P_2 is oriented with its pass plane making an angle β with respect to the X axis. The Jones matrix of P_2 is

$$\mathcal{P}(\beta)=\begin{pmatrix}\cos^2\beta & \cos\beta\,\sin\beta\\ \cos\beta\,\sin\beta & \sin^2\beta\end{pmatrix}. \tag{12}$$

The transmitted amplitude through the polarizer, considering Eqs. (9) and (12), is

$$\begin{pmatrix}A_x''\\ A_y''\end{pmatrix}=\mathcal{P}(\beta)\begin{pmatrix}A_x'\\ A_y'\end{pmatrix}. \tag{13}$$

Then, the readout intensity $I_c(x,\beta)=|A_x''|^2+|A_y''|^2$ becomes

$$I_c(x,\beta)=\tfrac{1}{2}\,[1-\cos 2\Delta(x)\,\cos 2\beta - \sin 2\Delta(x)\,\sin 2\beta\,\cos\psi(x)]. \tag{14}$$

Finally, the incoherent input $I_i(x)$ has been converted to a coherent output $I_c(x,\beta)$, where the parameter β governs the contrast, as will be detailed in the next section.

3 Experimental Results

A BSO crystal of dimensions $L_x=L_y=10$ mm and $L_z=3$ mm was utilized and a voltage $V=9$ kV was applied between their (110) faces. The intensity of the incoherent grating source was less than 1 mW/cm^2, and a 5-mW He-Ne laser ($\lambda=633$ nm) was employed for the readout beam. The measured rotatory power was $\rho=22$ deg/mm. For the calculation we used[8] $n_0=2.54$, $r_{41}=3.5$ pm/V.

A Ronchi grating of period $d=4$ lines/mm was used as the input transparency. Lens L_2 ($f/6$) images the grating in the crystal with unit magnification. The intensity distribution received in the crystal plane is

$$I_i(x)=I_0\left(\frac{1}{2}+\sum_{m=1}^{\infty}\frac{\sin(\pi m/2)}{\pi m/2}\cos\left(2\pi m\,\frac{x}{d}\right)\right)\operatorname{rect}\left(\frac{x}{L_x}\right), \tag{15a}$$

and the normalized light intensity is

$$t(x)=I_i(x)/I_0. \tag{15b}$$

According to Eq. (7), the received intensity distribution $I_i(x)$ is encoded as a birefringence modulation. In this case, by using Eqs. (4) and (5), the total internal field becomes

$$E(x)=\begin{cases} E_1=\dfrac{2V}{L_x}\left(\dfrac{1+G}{2+G}\right) & \text{if } I_i(x)=0,\\[2ex] E_2=\dfrac{2V}{L_x}\left(\dfrac{1}{2+G}\right) & \text{if } I_i(x)=I_0. \end{cases} \tag{16}$$

Usually $G\gg 1$, and the expression for $E(x)$ reduces to

$$E(x)=\begin{cases} E_1\approx\dfrac{2V}{L_x}=2E_a & \text{if } I_i(x)=0,\\ E_2\approx 0 & \text{if } I_i(x)=I_0. \end{cases} \tag{17}$$

Consider again the intensity received by the crystal, described by Eq. (15a). The periodically striped illuminated regions [$I_i(x)=I_0$] alternate with dark regions of the same width [$I_i(x)=0$]. It follows from Eq. (17) that in the bright striped areas the total internal field drops to a negligible value in comparison with the magnitude of the field in the dark regions, which will increase beyond the external applied value E_a. As a consequence, in view of Eq. (7), the induced birefringence tends to zero in the illuminated regions, while maintaining a nonnegligible value in the dark stripes, that is,

$$\delta n(x)=\begin{cases} \delta n_1=r_{41}n_0^3(2E_a) & \text{if } I_i(x)=0,\\ \delta n_2=0 & \text{if } I_i(x)=I_0. \end{cases} \tag{18}$$

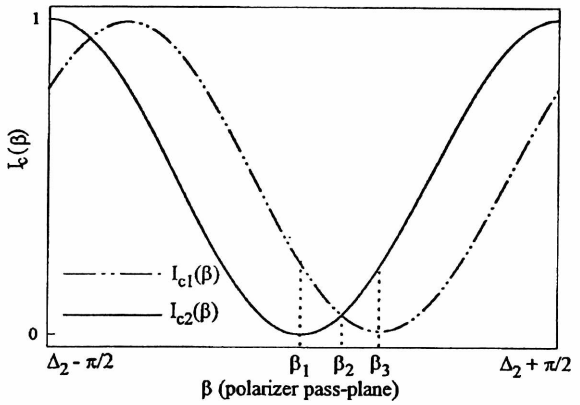

Fig. 2 Transmitted intensity of the polarizer P_2 for the components $I_{c1}(\beta)$ (elliptically polarized) and $I_{c2}(\beta)$ (linearly polarized).

It is clear that $\delta n(x)$ has the same spatial period as $I_i(x)$.

Also, by using Eqs. (10), (11), and (17) we have

$$\varphi(x)=\begin{cases} \varphi_1=\dfrac{2\pi}{\lambda}\,\delta n_1 & \text{if } I_i(x)=0,\\ \varphi_2=0 & \text{if } I_i(x)=I_0, \end{cases} \tag{19a}$$

$$\psi(x)=\begin{cases} \psi_1=\tan^{-1}\left(\dfrac{\varphi_1}{2\rho}\right) & \text{if } I_i(x)=0,\\ \psi_2=0 & \text{if } I_i(x)=I_0, \end{cases} \tag{19b}$$

and

$$\Delta(x)=\begin{cases} \Delta_1=L_z\left[\rho^2+\left(\dfrac{\varphi_1}{2}\right)^2\right]^{1/2} & \text{if } I_i(x)=0,\\ \Delta_2=L_z\rho & \text{if } I_i(x)=I_0. \end{cases} \tag{19c}$$

Thus, when the linearly polarized collimated readout beam propagates through the crystal, it will emerge periodically modulated in its ellipticity. Those parts of the readout beam that pass through the crystal regions where $\delta n\approx 0$ will emerge linearly polarized with the plane of polarization rotated an angle $\Delta_2=\rho L_z$ with respect to that of the entering light. The remaining part of the emerging wave will be elliptically polarized, because it has traveled through the periodic stripes where δn is not negligible (write-in dark regions).

Returning to Eq. (14), we have

$$I_c(x,\beta)=\begin{cases} I_{c1}(\beta)=\tfrac{1}{2}\,(1-\cos 2\Delta_1\,\cos 2\beta-\sin 2\Delta_1 \times\sin 2\beta\,\cos\psi_1) & \text{if } I_i(x)=0,\\ I_{c2}(\beta)=\tfrac{1}{2}\,(1-\cos 2\Delta_2\,\cos(2\beta)-\sin 2\Delta_2 \times\sin 2\beta) & \text{if } I_i(x)=I_0. \end{cases} \tag{20}$$

This expression analyzes the transmitted intensity of polarizer P_2 into two parts: a linearly polarized part of the readout wavefront exiting the crystal, $I_{c2}(\beta)$, and an elliptically polarized part, $I_{c1}(\beta)$. Figure 2 shows $I_{c1}(\beta)$ and $I_{c2}(\beta)$. The phase shift between them depends on the value of δn_1. Then $I_c(x,\beta)$ can be rewritten as

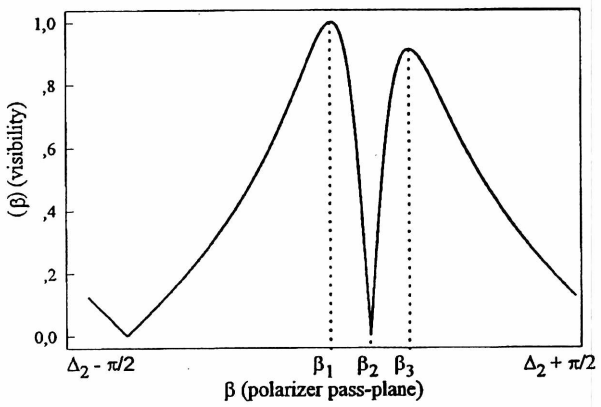

Fig. 3 Visibility of the coherent readout image.

$$I_c(x,\beta)=I_{c2}(\beta)t(x)+I_{c1}(\beta)t\left(x\pm\frac{d}{2}\right). \tag{21}$$

Consider the case $\beta=\beta_1=\Delta_2=L_z\rho$. It means that when the external applied voltage is off ($V=0$), the system is in extinction and no light passes through the analyzer P_2. But if $V\neq 0$, taking into account Eqs. (20) and (21), the following emerging readout intensity results:

$$I_c(x,\beta_1)=I_{c1}(\beta_1)t\left(x\pm\frac{d}{2}\right). \tag{22}$$

That is, the emerging wave of the readout beam will be alternately polarized linearly and elliptically with period d. The analyzer P_2 will block out the linearly polarized parts and will select a component of the elliptically modulated portion of the wavefront. Alternate dark and bright stripes will exit the polarizer. In this way, a coherent contrast-reversed replica of the input is obtained, converting the modulation of birefringence into modulation of transmission. Let us suppose that the spatial coherence of the readout beam is high and that free propagation takes place. In this case the Fresnel intensity distribution along the Z axis will be the same as if the original transparency, shifted a half period, had been located at the position of the polarized P_2.

The visibility of the readout coherent image $I_c(x,\beta)$, defined as

$$\mathscr{V}(\beta)=\left|\frac{I_1(\beta)-I_2(\beta)}{I_1(\beta)+I_2(\beta)}\right|, \tag{23}$$

is displayed in Fig. 3, where it can be observed that the absolute maximum, $\mathscr{V}(\beta)=1$, is reached, because $I_2(\beta_1)\cong 0$.

Let us impose the condition $\mathscr{V}(\beta)=0$. According to the expression (23), this implies equality of the linear and the elliptical components transmitted. The value of β that fulfills this constraint is

$$\beta=\beta_2=\tfrac{1}{2}\tan^{-1}\left(\frac{\cos 2\Delta_1-\cos 2\Delta_2}{\sin 2\Delta_2-\sin 2\Delta_1\cos\psi_1}\right). \tag{24}$$

In this case, taking into account that $t(x+d/2)\cong 1=t(x)$, we obtain

$$I_c(x,\beta_2)=C, \tag{25}$$

so that the output of the polarizer P_2 is uniform.

Another important value of β is that for which $I_{c1}(\beta)$ is minimum. From this condition, $\partial I_{c1}(\beta)/\partial\beta=0$, we have

$$\beta=\beta_3=\tfrac{1}{2}\tan^{-1}(\tan 2\Delta_1\cos\psi_1). \tag{26}$$

Then

$$I_c(x,\beta_3)=I_{c1}(\beta_3)t\left(x+\frac{d}{2}\right)+I_{c2}(\beta_2)t(x). \tag{27}$$

By considering Fig. 2 it is clear that $I_{c1}(\beta_3)\ll I_{c2}(\beta_3)$ and Eq. (27) can be written as:

$$I_c(x,\beta_3)\approx I_{c2}(\beta_3)t(x). \tag{28}$$

In this case, a direct-contrast output is obtained.

As β is rotated from β_1 to β_3, more and more of the linearly polarized parts of the light emerging from the crystal will be transmitted through the analyzer P_2, and less and less of the elliptically polarized parts will be transmitted.

In the three coherent readout images of Fig. 4 the polarizer P_2 was oriented at $\beta=\beta_1$ and the registers were obtained for different longitudinal positions under free propagation. In the following, all distances are measured from the crystal plane. Figure 4(a) displays a contrast-reversed

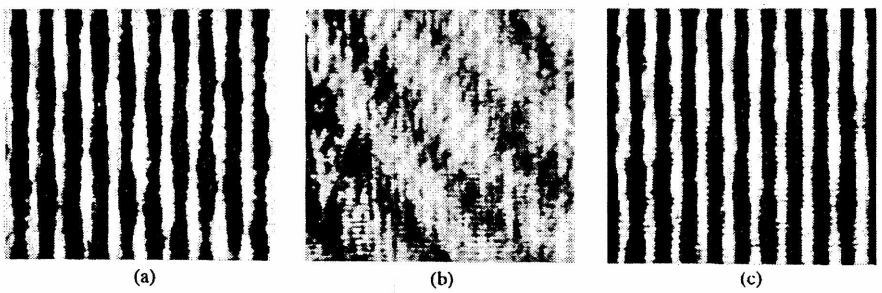

Fig. 4 Self-imaging outputs with the polarizer P_2 oriented at $\beta=\beta_1$: (a) $z=z_T$, (b) $z=5z_T/4$, and (c) $z=3z_T/2$.

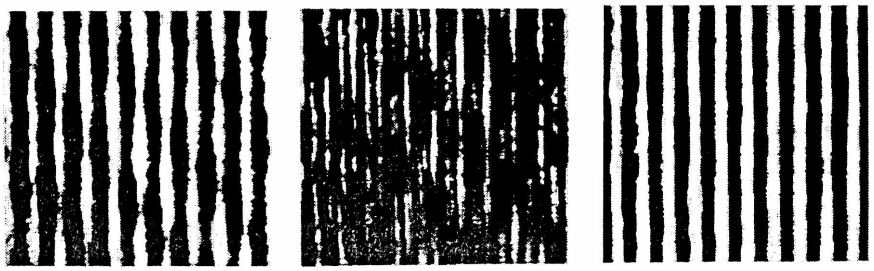

(a) (b) (c)

Fig. 5 Coherent readout images at $z=z_T$ with the pass plane of the polarizer P_2 set at (a) $\beta=\beta_1$, (b) $\beta=\beta_2$, and (c) $\beta=\beta_3$.

self-image registered at a distance z_T. Figure 4(b) corresponds to a defocused plane located at $5z_T/4$, while Fig. 4(c) displays a reverse-contrast image with respect to Fig. 4(a) and is obtained at a distance $3z_T/2$.

The pictures displayed in Fig. 5 were registered at the distance z_T for three values of the angle β. Figure 5(a) displays a contrast-reversed self-image obtained when the angle $\beta=\beta_1$. In Fig. 5(b) a defocused image is registered by setting the angle $\beta=\beta_2$, and in Fig. 5(c) a direct-contrast self-image was read out with the angle $\beta=\beta_3$.

By comparison of Fig. 4(a), 4(b), 4(c) with Fig. 5(a), 5(b), 5(c), respectively, it can be seen that a given longitudinal displacement could be comparable to a certain value of β at a fixed plane.

The sequence of Fig. 6 was obtained for values of $\beta=\beta_1,\beta_2,\beta_3$ respectively, in a plane located at $5z_T/4$ from the crystal. This would be comparable to obtaining three registers at distances $z_T/4$ apart from each other, for instance $5z_T/4$, $6z_T/4$, and $7z_T/4$, at a fixed value of $\beta=\beta_1$.

4 Discussion and Conclusions

By observing the visibility curve it can be concluded that an interesting domain runs from β_1 to β_3. To a high-contrast distribution at $\beta=\beta_1$ corresponds a reverse high-contrast version at $\beta=\beta_3$. This could be very useful in certain applications. The converter itself can be planned as a subsystem of an optical device in which control of the visibility is a key point for subsequent processing. In order to achieve this situation, the condition established by Eq. (28) must be fulfilled. This implies a high eccentricity of the elliptical light that originates the component $I_{c1}(\beta)$ [see Eq. (20)], implying a low value for δn_1. As δn_1 increases, $\Delta\beta=\beta_3=\beta_1$ and $I_{c1}(\beta_3)$ increase as well, the visibility in $\beta=\beta_3$ decreases, and this diminishes the system's ability to reverse the contrast of the grating encoded at $\beta=\beta_1$. Let us suppose that the appropriate conditions are fulfilled. Then, for instance, let us suppose that a reference Ronchi grating is placed beyond the polarizer P_2. Hence, the moiré pattern that arises between a readout self-image and a reference grating can be employed to detect phase objects.[9] Furthermore, the contrast control of the self-images could contribute to the easy visualization of those objects. Also, if a birefringent material is located between the analyzer and the reference grating, the shift in the moiré fringes can be used for quantitative determination of the birefringence.

In some circumstances, for subsequent processing, it could be useful to have a Talbot object in the form of an incoherent input, that is, a TV picture, 2-D array, etc. In this case, an incoherent-to-coherent converter as was proposed in this paper could be appropriate.

Some constraints arise from the nature of the converter. It is limited by the crystal response time, which depends on the intensity of the input signal. Furthermore, geometric resolution limitations arise from the write-in imaging system. Also, a compromise must be considered between the increasing of the crystal thickness to improve the sensitivity and the corresponding constraints on the spatial resolution that result. According to the experimental conditions detailed at the beginning of the previous section, the available resolution was 20 lines/mm. Certainly, that can be improved several fold by reducing the crystal thickness (L_z)

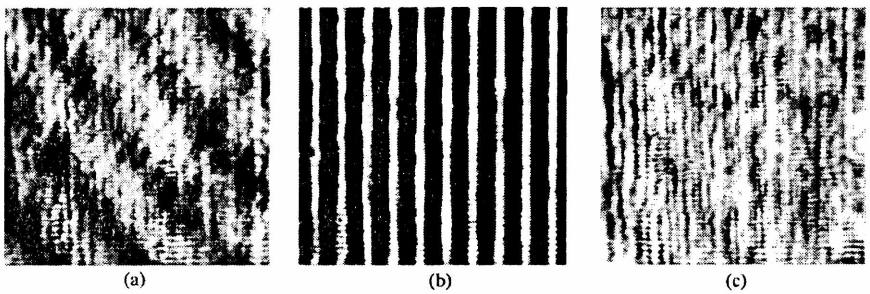

(a) (b) (c)

Fig. 6 Coherent readout images at $z=5z_T/4$ with the pass plane of the polarizer P_2 set at (a) $\beta=\beta_1$, (b) $\beta=\beta_2$, and (c) $\beta=\beta_3$.

and increasing the f number of lens L_2. On the other hand, it should be mentioned that because of the finite crystal dimension L_x, the diffracted high harmonics in the readout process gradually "walk off" the zero-order beam and do not take part in the image formation. This inherent drawback in any self-imaging process limits a complete replication of the input.

Finally, we should emphasize the nonholographic nature of the converter, which represents an experimental advantage. A device such as a photorefractive incoherent-to-coherent optical converter (PICOC) could be employed as well, but it has a holographic support[10] that considerably complicates the experimental arrangement. Besides, it lacks flexibility for controlling the contrast of the output.

Acknowledgments

M. C. Lasprilla acknowledges an external fellowship of CONICET (Argentina) and financial support from COLCIENCIAS (Colombia). M. Tebaldi acknowledges an internal fellowship of CONICET. This work was supported by PID 3974/92 of CONICET.

References

1. K. Patorski, "The self-imaging phenomenon and its applications," in *Progress in Optics*, Vol. XXVII, E. Wolf, Ed., Chap. 1, pp. 3–45, North-Holland, Amsterdam (1989).
2. W. Montgomery, "Self-imaging objects of infinite aperture," *J. Opt. Soc. Am.* **57**, 772–778 (1967).
3. R. F. Edgar, "The Fresnel diffraction image of periodic structures," *Opt. Acta* **16**, 281–287 (1969).
4. J. P. Huignard and P. Günter, "Optical processing using wave mixing in photorefractive crystals," in *Photorefractive Materials and Their Applications II*, P. Günter and J. P. Huignard, Eds., Chap. 6, pp. 205–271, Springer-Verlag, Berlin (1989).
5. P. Günter and J. P. Huignard, "Photorefractive effects and materials," in *Photorefractive Materials and Their Applications I*, P. Günter and J. P. Huignard, Eds., Chap. 2, pp. 7–73, Springer-Verlag, Berlin (1989).
6. L. Liu and X. Liu, "Opto-optical switching using field enhancing effect in $Bi_{12}SiO_{20}$," *J. Appl. Phys.* **72**(2), 337–343 (1992).
7. A. Gerrad and J. M. Burch, "Matrices in polarization optics," in *Introduction to Matrix Methods in Optics*, Chap. 4, pp. 179–239, Wiley, London (1975).
8. P. Günter and H. J. Eichler, "Introduction to photorefractive materials," in *Electro-Optical Effects in Dielectric Crystals*, P. Günter, Ed., Part I p. 12, Springer-Verlag, Berlin (1987).
9. J. Ibarra and J. Ojeda Castañeda, "Talbot interferometry: a new geometry," *Opt. Comm.* **96**, 294–301 (1993).
10. A. Marrakchi, A. R. Tanguay, Jr., J. Yu, and D. Psaltis, "Physical characterization of the photorefractive incoherent-to-coherent optical converter," *Opt. Eng.* **24**(1), 124–131 (1985).

María del Carmen Lasprilla A. completed her MS in physics with a specialization in optics in the Department of Physics, Universidad Industrial de Santander, Colombia, in 1989. She is currently an assistant professor in the same department. She is also a PhD student at the Universidad Nacional de La Plata and does research at Centro de Investigaciones Opticas, Argentina. Her research includes photorefractive devices and optical signal processing.

Alexandra Agra Amorim received a degree in physics (optoelectronics) in 1990 from the University of Porto, Portugal. She held a scholarship at JNICT (CERN project) for 2 years (1990–1992). She has done research at the Vrije Universiteit Brussel and Centro de Investigaciones Opticas. She is preparing the presentation of an MS thesis on nonlinear processing with BSO crystals. She is an assistant in the Physics Department of the Engineering Institute of Porto.

Myrian Cristina Tebaldi received her MS degree from the Universidad Nacional de La Plata in 1994. She teaches physics and is a PhD student at the same university. She is involved in research on real-time image processing at Centro de Investigaciones Opticas, Argentina.

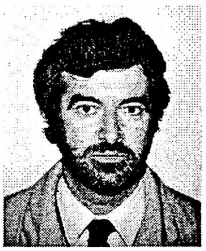

Néstor A. Bolognini obtained his PhD in physics from the Universidad Nacional de La Plata, Argentina, in 1981. He joined the Centro de Investigaciones Opticas in La Plata in 1977. He did research at the University of Stuttgart and Universidad Autónoma de Madrid. His research activities have included speckle techniques, holography, and Fourier optics. He is now involved in image processing using photorefractive materials. He is currently a researcher of CONICET (Nacional Research Council of Argentina), a professor of physics at Universidad Nacional de La Plata, and a PhD thesis adviser.